Replenishment of mitochondrial Na$^+$ and H$^+$ by ionophores potentiates cutaneous wound healing in diabetes

Liangliang Bai [a,1], Linping Wu [b,1], Changsheng Zhang [c], Zhiwen Liu [d], Liang Ma [c], Jing Ni [b], Dezhen He [b], Mingxuan Zhu [e], Shaoyong Peng [e,f,g], Xiaoxia Liu [e,g], Huichuan Yu [e,g], Yuhe Lei [h], Yanxin Luo [e,f,g], Yu Zhang [e], Xiaolin Wang [e,g,***], Gang Wei [a,**], Yingjie Li [b,*]

[a] School of Pharmaceutical Sciences, Guangzhou University of Chinese Medicine, Guangzhou, China
[b] Center for Chemical Biology and Drug Discovery, Guangzhou Institutes of Biomedicine and Health, Chinese Academy of Sciences, Guangzhou, China
[c] Key Laboratory of Tropical Marine Bioresources and Ecology, Guangdong Key Laboratory of Marine Materia Medica, South China Sea Institute of Oceanology, Chinese Academy of Sciences, Guangzhou, China
[d] Department of Molecular and Cellular Biology, Baylor College of Medicine, Houston, USA
[e] Guangdong Institute of Gastroenterology, Guangdong Provincial Key Laboratory of Colorectal and Pelvic Floor Disease, The Sixth Affiliated Hospital, Sun Yat-sen University, Guangzhou, China
[f] Department of General Surgery, The Sixth Affiliated Hospital, Sun Yat-sen University, Guangzhou, China
[g] Biomedical Innovation Center, The Sixth Affiliated Hospital, Sun Yat-sen University, Guangzhou, China
[h] Department of Pharmacy, Shenzhen Hospital of Guangzhou University of Chinese Medicine, Shenzhen, China

ARTICLE INFO

ABSTRACT

Diabetic foot ulcer (DFU) is a highly morbid complication in patients with diabetes mellitus, necessitating the development of innovative pharmaceuticals to address unmet medical needs. Sodium ion (Na$^+$) is a well-established mediator for membrane potential and osmotic equilibrium. Recently, Na$^+$ transporters have been identified as a functional regulator of regeneration. However, the role of Na$^+$ in the intricate healing process of mammalian wounds remains elusive. Here, we found that the skin wounds in hyponatremic mice display a hard-to-heal phenotype. Na$^+$ ionophores that were employed to increase intracellular Na$^+$ content could facilitate keratinocyte proliferation and migration, and promote angiogenesis, exhibiting diverse biological activities. Among of them, monensin A emerges as a promising agent for accelerating the healing dynamics of skin wounds in diabetes. Mechanistically, the elevated mitochondrial Na$^+$ decelerates inner mitochondrial membrane fluidity, instigating the production of reactive oxygen species (ROS), which is identified as a critical effector on the monensin A-induced improvement of wound healing. Concurrently, Na$^+$ ionophores replenish H$^+$ to the mitochondrial matrix, causing an enhancement of mitochondrial energy metabolism to support productive wound healing programs. Our study unfolds a new role of Na$^+$, which is a pivotal determinant in wound healing. Furthermore, it directs a roadmap for developing Na$^+$ ionophores as innovative pharmaceuticals for treating chronic dermal wounds in diabetic patients.

1. Introduction

Chronic wounds, such as diabetic foot ulcer (DFU), are a prevalent and highly morbid complication arising from diabetes mellitus. Among the estimated 537 million individuals with diabetes, 19–34 % will develop DFU during their lifetime [1]. The healing of chronic wounds in diabetes is obstinate, mainly due to repairing cell generation disorder and peripheral vascular damage under the hyperglycemic milieu [2]. Presently, several therapeutic solutions are available for the

management of diabetic wounds, such as debridement, revascularization, infection prevention care, and bioengineered skin substitutes [3,4].

Abbreviations

PMDF	primary mouse dermal fibroblasts
A/O	antimycin A plus Oligomycin A
ING-2	ION NaTRIUM Green-2 AM
NAO	acridine orange 10-nonyl bromide
TMRE	tetramethylrhodamine ethyl ester
PC	phosphatidylcholine

Nevertheless, the majority of these therapies are limited by the intricate pathogenesis of chronic wounds and their poor curative effect in clinical practice [5]. This actuality desiderates the development of versatile therapeutic strategies that encompass repairing cell motivation and angiogenesis improvement to address the unmet medical needs in diabetic wound care.

Sodium ion (Na^+) is a well-defined mediator of membrane potential and osmotic equilibrium that presents conservatively across all cell types, controlling multiple cellular behaviors, such as proliferation, migration, differentiation, and directional polarization [6,7]. Bioelectrical networks mediated by Na^+ have been identified to be crucial for handling morphogenetic information, thereby influencing large-scale cell growth and tissue morphology jointly [8]. Emerging evidence sheds light on a new role of Na^+ that tightly links to regeneration. It has been reported that an early surge in transient Na^+ current in the wound vicinity of *Xenopus laevis* is required to initiate tail regeneration [9]. Multiple sodium channels have recently been identified as determinants in *Drosophila melanogaster* wing regeneration [10]. Those cumulative studies illustrate the exemplary role of Na^+ in the regenerative microenvironment, resembling a niche conducive to wound healing. Nevertheless, the specific role of Na^+ in the injury-response of mammals, which are highly regeneration-incompetent, still needs to be defined, and much less is known about its underlying molecular mechanisms.

Mitochondrion is a special organelle primarily recognized for its production of ATP that serves as the universal energy source for the cell. Nevertheless, it is noteworthy that all mitochondria also generate heat. The uncoupling of the H^+ current across the inner mitochondrial membrane (IMM) but do not generate ATP is referred to as H^+ leak, letting energy dissipate as heat [11]. The mechanisms of mitochondrial H^+ leak remained largely unknown. The mitochondrial H^+ leak can be pharmacologically induced by employing chemical protonophores. For instance, 2,4-dinitrophenol (DNP), a membrane-soluble weak acid, can induce H^+ leakage by freely transporting H^+ across the IMM [12]. Indeed, DNP can increase the metabolic rate of mitochondria, shifting the energy balance toward expenditure [11]. This mechanism endows its remarkable efficacy against type 2 diabetes, fatty liver disease, and metabolic syndrome in animal models [13]. Mitochondrial dysfunction is a hallmark of type 2 diabetes [14]. Thus, when the pace of mitochondrial metabolism is expedited by artificially promoting mitochondrial H^+ leak, it may benefit to restore the physiological function of cells in devastating high-glucose microenvironment.

In this work, we develop a multifunctional strategy for diabetic wound treatment, by which manually co-replenishing mitochondrial Na^+ and H^+ using Na^+ ionophores. This appealing pharmaceutical approach displays an appealing therapeutic effect on cutaneous wound healing in mouse models. Our study highlights a novel, feasible, and economic therapy to effectively manage chronic wounds in diabetes.

2. Materials and methods

2.1. Cell lines and cell culture

HACAT, an immortalized human keratinocyte cell line derived from skin tissue and spontaneously transformed into immortalized human keratinocytes after long-term culture [15], was purchased from the National Collection of Authenticated Cell Cultures (Shanghai, China). Short tandem repeat (STR) profiling was employed to identify this cell line at nine different loci (Amelogenin: X; CSF1PO: 9; D13S317: 10; D16S539: 9; D5S818: 12; D7S820: 9; THO1: 9,3; TPOX: 11; vWA: 16). HEK293, 293T, mouse embryonic fibroblasts (MEF), and primary umbilical vein endothelial cells (HUVEC) were derived from the American Type Culture Collection (Gaithersburg, MD, USA). Primary mouse dermal fibroblasts (PMDF) were isolated, as previously described [16], from 1 to 3 days newborn KM mice (Vital River, Beijing, China) with validation of positive vimentin phenotype. All cell lines were detected for mycoplasma periodically. HACAT, MEF, and PMDF were cultured in DMEM medium complemented with 10 % (v/v) fetal bovine serum (FBS), GlutaMax supplement (2 mM), and sodium pyruvate (1 mM). HEK293 and 293T were grown in EMEM medium with 10 % (v/v) FBS. All cell lines were maintained in an incubator at 37 °C with 5 % CO_2.

We depleted mitochondria in HACAT cells through enforced mitophagy [17]. PARK2 gene (NM_004562.2) encoding Parkin, a component of a multiprotein E3 ubiquitin ligase complex that targets mitochondrion for proteasomal degradation, were embedded in a viral expression vector. Lentiviral particles were generated by co-transfecting the Parkin-expressed vector with packaging plasmids psPAX2 and pMD2G into 293T cells, similar to our previous description [18]. HACAT cells were infected with the lentivirus in the presence of polyethyleneimine, and positive clones were screened out using puromycin. We used carbonyl cyanide 3-chlorophenylhydrazone (CCCP) or Antimycin A plus Oligomycin A (A/O) to induce mitochondrial dysfunction and efficiently enforce widespread mitochondrial depletion by detecting the expression of mitochondrial proteins HSP60. A uridine supplement was added to the medium for culturing mitochondria-depleted cells [17].

2.2. Reagents

Detailed information about the reagents used in this study is presented in Table S1.

2.3. Cell viability assay

Cell Counting Kit-8 (CCK-8) was used to perform the cell viability assay with standard protocols, as reported previously [19]. We complied a two-fold dilution method to dilute ionophores for treating cells for 72 h.

2.4. Animal studies

BALB/c mice were purchased from the Vital River (Beijing, China). DB/DB mice (Gempharmatech, Jiangsu, China) carrying diabetes and obesity phenotype have been reported previously [20]. All mice were maintained under a specific pathogen-free (SPF) laboratory animal barrier system. Mice were fed with salt-uncontrolled diet (0.5 % NaCl, Xietong, Jiangsu, China) or salt-controlled diet (0.04 % and 0.01 % NaCl, w/w, Xietong, Jiangsu, China) for 10 weeks to establish a hyponatremic model. We tracked body weights and validated the serum Na^+ levels using a colorimetric method-based blood sodium assay kit. To establish an *in vivo* model for full-thickness skin wound healing assessment, we generate excisional wounds in the back of mouse skin using sterile biopsy punches (5 mm). Agents diluted in phosphate buffer saline were dropped into the wounded cavity, and wounds were finally splinted with Tegaderm (3 M) sterile transparent dressing. The

quantified wound area was normalized to peripheral punched silica. Wound tissue samples were sectioned and fixed with paraformaldehyde, then stained with haematoxylin and eosin (H&E), immunofluorescence, or Masson's trichrome by the Servicebio (Wuhan, China) using standard procedures. Sections were scanned by a high-throughput whole-slide scanning system (Qiangsheng, Shenzhen).

2.5. Serum and intracellular Na^+ detection

We employed a potassium pyroantimonate-based serum sodium assay kit to detect mice fed with the Na^+-controlled diet. A 10-fold dilution was performed to precipitate proteins in mouse serum using ethanol. The collected supernatant was mixed with a working solution containing detected regent (1 mL per sample) and ethanol (100 μL) for 5 min at room temperature. A microplate reader read each sample's optical density (520 nm).

A Na^+-sensitive fluorescent dye, ION NaTRIUM Green-2 AM (ING-2), was used to evaluate cellular Na^+ content. Cells grown in 96-well plates with a density of 20,000 cells per well were treated with ionophores at indicated concentrations and then loaded with the probe (5 μM) for 1 h. After loading, cells were washed gently twice with cold PBS, intracellular ING-2 was excited by an Ar laser (488 nm), and a microplate reader recorded its emission fluorescence (550 nm). Additionally, we employed a laser scanning confocal microscope (Carl Zeiss, Oberkochen, Germany) to image the ING-2 fluorescence in cells treated with monensin A (125 nM) for 30 min.

2.6. The chicken chorioallantoic membrane model

The model was established according to the published protocols [21]. Briefly, fertilized eggs were kept at 37 °C in a humidified incubator for 5 days. A hole of approximately 3 cm in diameter was created in the eggshell. Monensin A solution was injected into the cavity under the chorioallantoic membrane for 24 h. The growing vessels were captured using a camera, and the number of vessels was quantified to assess the efficacy of monensin A on vascular growth.

2.7. Scratch wound healing assay

Cells were seeded in a 2-well silicone insert (Cat# 81176, Ibidi) with a defined cell-free gap, followed by the monensin A-treatment in a low-FBS (1 %) medium. The dynamic scratch wound of cells was monitored by an IncuCyte system.

2.8. Western blotting

Western blotting analysis was performed with standard protocols [19].

2.9. Fluorescence recovery after photobleaching (FRAP)

Monensin A (125 nM) was added to treat HACAT and HEK293 cells. Cells were labeled with acridine orange 10-nonyl bromide (NAO), and the membrane fluidity was evaluated through a FRAP experiment similar to our previous description [22]. Briefly, intracellular NAO was excited with an argon/krypton laser using an excitation wavelength of 488 nm, detecting its emission at 525 nm. The selected areas of NAO fluorescence were bleached using 15 scans at 20 % laser power. We then recorded 40–60 scans (HACAT: 57 scans; HEK293: 43 scans) with 1 s per scan to quantify the recovered fluorescence intensity after photobleaching.

2.10. Reactive oxygen species (ROS) detection

HACAT and HEK293 cells were treated with ionophores for the indicated times. Intracellular ROS was detected by treating with 2′,7′-Dichlorodihydrofluorescein diacetate (H_2DCFDA, 10 μM), following the standard procedures described previously [23].

2.11. Bulk RNA-sequencing and RT-qPCR

HACAT cells were incubated with monensin A (60 nM) for 3 h. Total RNA was extracted using a column-based total RNA purification kit following its recommended protocols. RNA samples were submitted to LC Sciences (Hangzhou, China) for bulk RNA sequencing using the Illumina platform. In the validated study, we reversed the single-stranded RNA to cDNA using an RT Master Mix kit with gDNA remover. The RT-qPCR was performed in a master mix containing SYBR Green I, cDNA template, and targeted gene primers (Table S2).

2.12. Measurement of oxygen consumption

The oxygen consumption rate (OCR) of HACAT cells was measured using a Seahorse XF24 Analyzer (Agilent, Santa Clara, USA) referring to our published protocols [22]. Briefly, the cells grown in assay media were pre-incubated at 37 °C without CO_2 for 1 h to allow cells to settle. The OCR was accessed in the analyzer following an indicated procedure, using oligomycin A (1 μM), carbonyl cyanide 4-(trifluoromethoxy) phenylhydrazone (FCCP, 2 μM), rotenone (0.5 μM), and antimycin A (0.5 μM). We replaced FCCP with ionophores to evaluate the effect of these compounds on mitochondrial function. The OCR was normalized to the protein context and its baseline.

2.13. Mitochondrial membrane potential (MMP) measurement

HACAT cells seated in the 96-well plates were treated with ionophores for 3 h before staining. Tetramethylrhodamine ethyl ester (TMRE, 200 nM) was employed to stain cells at 37 °C for 30 min to quantify the mitochondrial membrane potential according to its fluorescent signaling recorded by a microplate reader.

2.14. Intracellular adenosine triphosphate (ATP) assay

The ATP assay kit was used to measure the intracellular ATP levels following its recommended procedures. The supernatant of cell lysis with cell debris removal was incubated with the substrate solution. The luminescence was recorded by a Microplate Reader using a dedicated luminescence module.

2.15. Mitochondria isolation and mitochondrial Na^+ detection

We used a mitochondria isolation kit to isolate crude mitochondria derived from HACAT cells. Briefly, cells were homogenized in a Teflon-glass homogenizer at 4 °C. The homogenate was centrifuged at a centrifugation rate of $1000 \times g$ for 10 min to discard particles of precipitation, followed by mitochondria collection procedures by reinforcing the centrifugation to $11,000 \times g$ for 10 min at 4 °C. In the quality testing, the washed pellet was lysed to detect the mitochondrial protein HSP60 and cytoplasmic protein β-actin. To measure the mitochondrial Na^+, we resuspended the isolated mitochondria granules in a mitochondrial stock solution containing a sodium salt ingredient. Mitochondrial pellets were treated with monensin A (1000 nM and 500 nM) for 20 min at 37 °C, and mitochondrial Na^+ was detected using the Na^+-sensitive probe ING-2.

2.16. Statistical analyses

An unpaired Student's *t*-test or one-way ANOVA with Tukey's multiple-comparison test was used, as described in the corresponding figure legends. All *P* values are two-sided, and statistical analyses were performed using a GraphPad Prism 7. In all figures, $*P < 0.05$, $**P < 0.01$, and $***P < 0.001$ indicate the statistical significance and $P > 0.05$

is considered to be no significance (ns). Data are displayed as the mean ± SD unless otherwise stated.

3. Results

3.1. Impact of hyponatremia on cutaneous wound healing in mice

The transient sodium (Na^+) current, regulated by voltage-gated sodium channels, has been identified as a crucial factor in *Xenopus laevis* tail regeneration [9]. We posited that this conservative membrane potential mediator might exhibit similar significance in the context of mammalian skin wound repair, a facet yet to be elucidated in mammals. Hence, we aimed to assess the impact of hyponatremia through dietary control on the dynamics of wound healing (Fig. 1A). Mice were fed with a low-salt diet (0.04 % and 0.01 % NaCl by weight) for a period of 10 weeks to induce marked hyponatremic symptom (Fig. 1B). Although a slight but significant weight loss was observed during the course of the low-salt diets, weights returned to normal levels prior to the initiation of full-thickness skin wounds (Fig. 1C). Remarkably, the morphology of the wounded skin exhibited a pronounced delay in the healing process in hyponatremic mice (Fig. 1D), indicating that severe hyponatremia, characterized by low serum Na^+ content, hinders the repair of mouse wounds.

3.2. Stimulation of cell growth through elevating intracellular Na^+

Cell proliferation constitutes a pivotal aspect of the orchestrated series of events in tissue repair script [24]. Epidermal keratinocyte expansion, a key facet of epimorphosis, entails a proliferation phase preceding the development of regenerative tissues during the healing of skin wounds [25]. Noteworthy medicaments in this context include epidermal growth factor (EGF) and Kangfuxin solution (a Chinese medicine), both known for their efficacy in accelerating

re-epithelialization during the skin wound repair process [26,27]. Our results demonstrate their capacity to enhance cell growth across various cell lines, including HACAT, HEK293, and MEF (Fig. 1E). Next, we investigated the impact of an elevated intracellular Na^+ on the cell proliferation by blocking the routine Na^+ expelling. HEK293 cells treated with sub-cytotoxic concentrations of ouabain, a well-established Na^+-K^+-ATPase inhibitor leading to intracellular Na^+ accumulation, exhibited a marked increase in proliferation (Fig. 1F, Fig. S1A). This outcome highlights the potential of enhancing intracellular Na^+ context as a promising strategy for augmenting cell proliferation. However, similar results were not replicated in HACAT cells (Fig. 1F, Fig. S1A), likely attributable to its comparatively low Na^+-K^+-ATPase expression compared to HEK293 (Fig. 1G, Fig. S1B). The available data from the Human Protein Atlas datasets (https://www.proteinatlas.org/ENSG00000163399-ATP1A1/tissue) further indicates that the expression of Na^+-K^+-ATPase is relatively low in skin tissues, thereby limiting its potential as a druggable target in epidermal wound healing.

3.3. Facilitation of Na^+ equilibration across cellular membranes by Na^+ ionophores

As an alternative approach, we set our sights on several well-known Na^+ ionophores, including monensin A, nanchangmycin, lasalocid, and salinomycin, recognized for their capacity to bind to Na^+ and freely transport the ion across lipid membranes (Fig. 2A, D, and F; Fig. S2A) [28–30]. The pseudocyclic structures of these ionophores anchor Na^+ through their polyether skeletons (Fig. 2A, D, and F) [31]. Consequently, exposure of HACAT and HEK293 cells to monensin A, a representative polyether ionophore, showed a discernible increase in intracellular Na^+ content (Fig. 2B and C). Similarly, other Na^+ ionophores, including nanchangmycin, lasalocid, and salinomycin, also remarkably elevated intracellular Na^+ levels in HACAT cells (Fig. 2E and G, Fig. S2B). Nigericin, a typical K^+ ionophore characterized by low Na^+ affinity
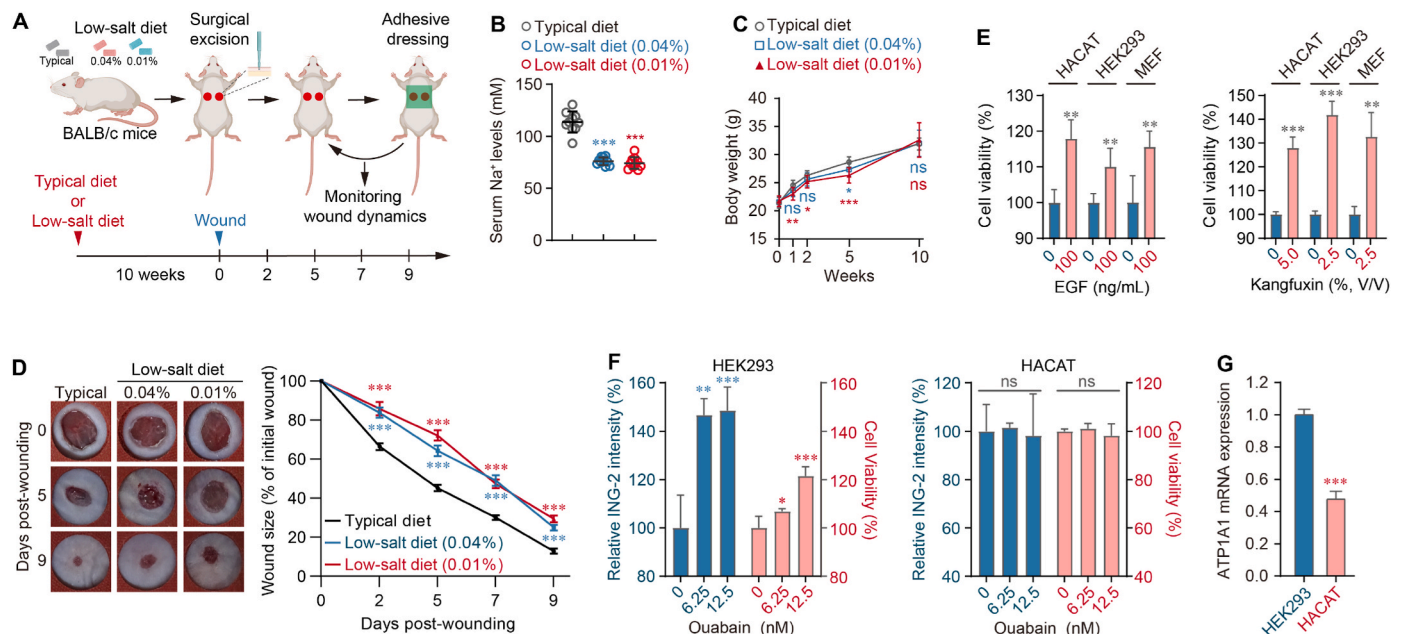
Fig. 1. Cutaneous wound exhibits a hard-to-heal phenotype in hyponatremic mice. (A) Schematic of full-thickness skin wounding on hyponatremic BLAB/c fed with salt-controlled diet (0.04 % NaCl and 0.01 % NaCl) or typical diet (0.5 % NaCl) for 10 weeks. (B) Serum Na^+ levels in the mice (n = 10 per group) after 10 weeks of salt-controlled diet. (C) Body weight of mice during the diet control. (D) The representative images (left) and wound healing dynamics (right) of mice (n = 8 per group) with low-sodium diets or typical diets. (E) Cell viability of HACAT, HEK293, and MEF cells incubated with EGF or diluted Kangfuxin solution for 72 h. (F) Intracellular Na^+ levels were detected by using a fluorescent probe (ING-2) in living HEK293 and HACAT treated with ouabain for 1 h. CCK-8-based cell viability assay on HEK293 and HACAT cells treated with ouabain for 72 h. (G) A comparison of ATP1A1 mRNA expression between HEK293 and HACAT. Data are represented as mean ± SD (E, F, G) or mean ± s.e.m (B, C). In all figures, *p < 0.05, **p < 0.01, ***p < 0.001, and "ns" indicates no significance (p > 0.05). Two-tailed Student's unpaired *t*-test (E, G); one-way ANOVA with Dunnett test (B, F; every mean versus control); two-way ANOVA with Sidak's multiple comparisons (C, D; low sodium diets versus normal diet, all time points).
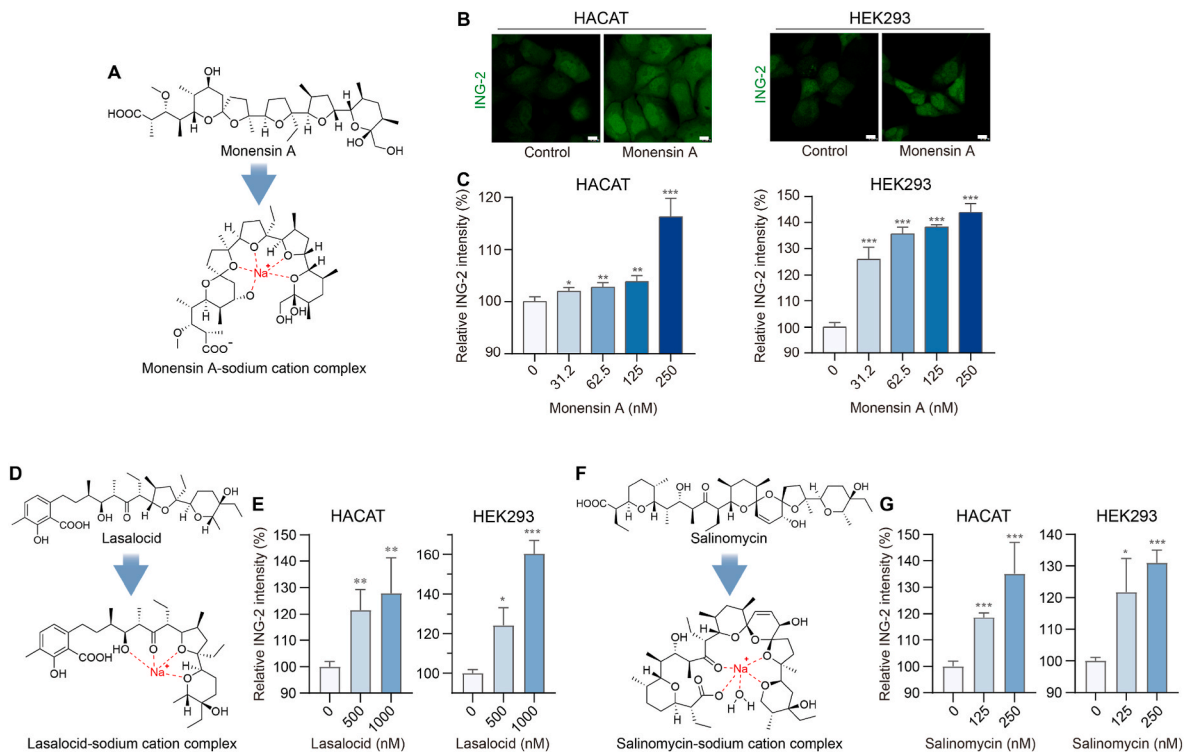
Fig. 2. Na$^+$ ionophores elevate intracellular sodium content. (A, D, F) Chemical structures and their matched sodium complexes of Na$^+$ ionophores, including monensin A (A), lasalocid (D), and salinomycin (F). (B, C) Confocal images (B) and microplate reader-based quantification (C) of intracellular Na$^+$ in monensin A-treated HACAT and HEK293 cells, which was probed by a fluorescent dye ING-2. Scale bar = 10 μm. (E, G) The quantification of intracellular Na$^+$ levels in HACAT and HEK293 cells treated with lasalocid and salinomycin for 1 h. Error bars are mean ± SD. One-way ANOVA with Dunnett test (C, E, G; every mean versus control).

(Fig. S2C) [32], did not elicit an increase in intracellular Na$^+$ levels in HACAT cells (Fig. S2D).

3.4. Monensin A exhibits versatile activities on facilitating proliferation, angiogenesis, and migration in vitro and ex vivo, and improves cutaneous wound healing in a mouse model

By assessing the proliferation-promoting capabilities of ionophores across various cell types, we observed a concentration-dependent increase in cell growth in HACAT and HEK293 cells treated with Na$^+$ ionophores (Fig. 3A). In line with its activity that does not affect intracellular Na$^+$ content, nigericin failed to stimulate cell proliferation in both HACAT and HEK293 cells (Figs. S3A and B). Among these Na$^+$ ionophores, monensin A demonstrated the ability to elevate intracellular Na$^+$ levels and stimulate cell proliferation in fibroblasts, including PMDF and MEF (Fig. S4 A, B; Fig. 3B). Additionally, monensin A did not solely promote the proliferation of HUVEC cells, it can also facilitate the tube formation of this vascular endothelial cell line (Fig. S4 C; Fig. 3C–E). This clue prompted an investigation into the potential pro-angiogenic property of monensin A. In a chick embryo chorioallantoic membrane model, monensin A-treated blood vessels displayed a more euangiotic morphology than the control (Fig. 3F and G). Additionally, monensin A accelerated scratched wound healing in monolayer HACAT cells within a short timeframe (20 h) of post-wounding (Fig. 3H), revealing an enhanced migration capacity of HACAT cells endowed by this ionophore.

Next, we employed a mouse-wounded surgical model to assess the potential of monensin A on enhancing wound healing *in vivo* (Fig. 3I). In BALB/c mice, the external application of monensin A significantly improved the dynamics of wound healing, resulting in faster closure compared to spontaneously healing wounds (Fig. 3J). In line, the mice wounds with monensin A treatment displayed a narrow width appearance with H&E staining (Fig. 3K). Importantly, histological sections of

the monensin A-treated tissues revealed a thicker granulation than the controlled wounds without monensin A incubation (Fig. 3K). These granulations were highly vascular, by which staining with the dual vascular endothelial markers CD31 and α-SMA (Fig. 3L). Furthermore, the Masson's trichrome staining confirmed an enhancement of collagen matrix in the bed of the wounds under monensin A external application (Fig. S5). Collectively, these findings highlight the multi-faceted functions of monensin A in pivotal processes that are critical for injury repair, encompassing proliferation, angiogenesis, and migration. As a consequence, these cumulative activities contribute to skin wound repair *in vivo*.

3.5. Monensin A triggers ROS production to enhance skin wound healing via reducing inner mitochondrial membrane (IMM) fluidity

In veterinary practice, ionophores supplementation has been demonstrated to improve energy metabolism [33], implying that mitochondria may be the target of these ionophores. To investigate the involvement of mitochondria in the proliferative effect induced by monensin A, we build a mitochondria-depleted HACAT cell line via boosting Pink1/Parkin-mediated mitophagy (Fig. 4A) [17]. Notably, the proliferative activity of monensin A was nullified in HACAT cells lacking mitochondria (Fig. 4B), indicating that the activities of this ionophore rely on mitochondrial function. Given that ionophores carrying Na$^+$ freely transport across both the plasma and mitochondrial membrane, we envisioned that monensin A elevates the mitochondrial Na$^+$ context. Accordingly, crude mitochondria isolated from HACAT cells revealed a substantial increase in Na$^+$ levels upon monensin A treatment (Fig. 4C and D). It has been established that mitochondrial Na$^+$ directly binds to phospholipids, such as phosphatidylcholine (PC) or PC–cardiolipin in the IMM, forming a Na$^+$-lipid complex that influences the IMM fluidity [34,35]. FRAP analysis using NAO, a lipophilic quenchable probe with a preference to bind cardiolipin enriched in the IMM [34,36], showed a
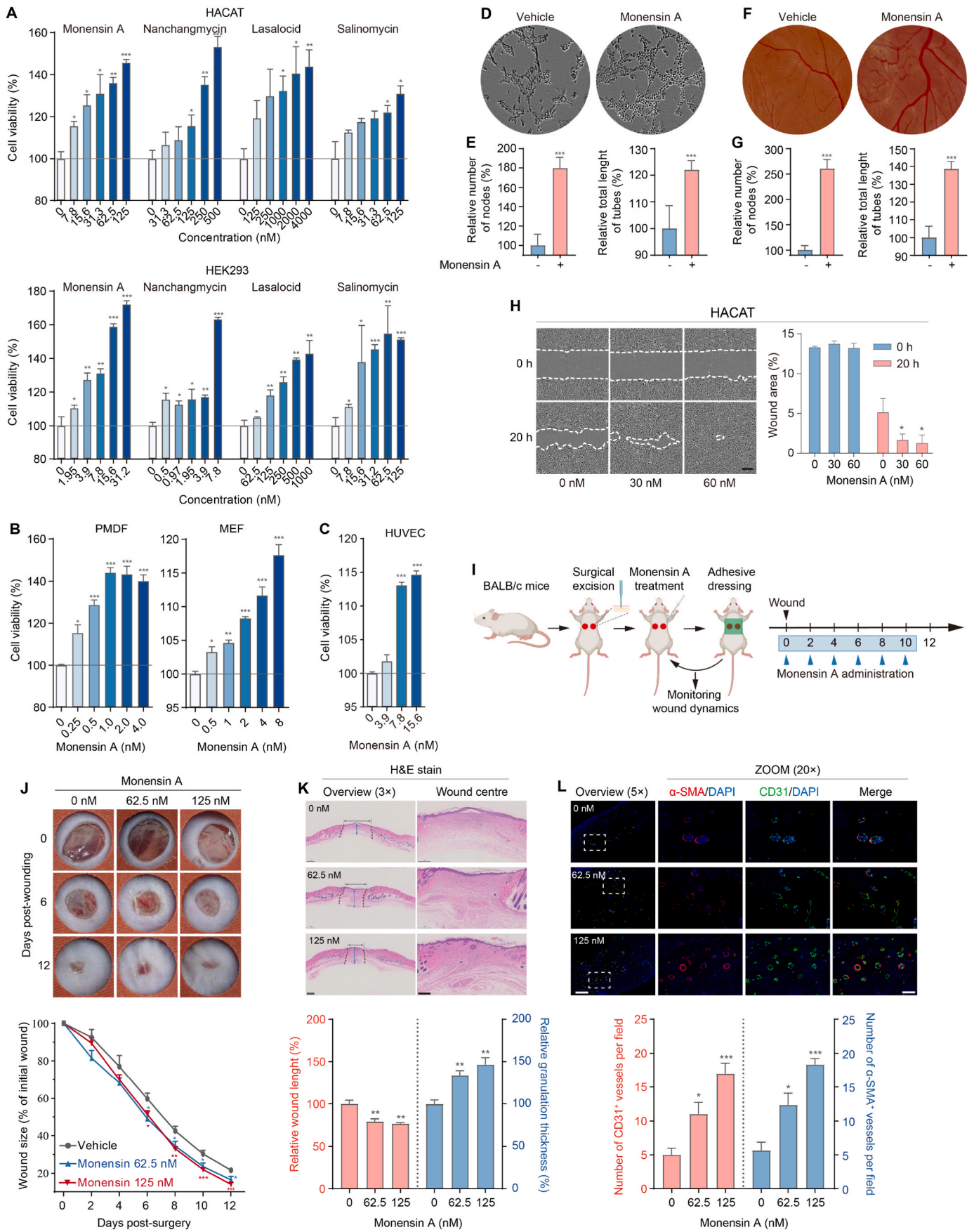
(caption on next page)

Fig. 3. Na$^+$ ionophores exhibit versatile activities on cell proliferation, angiogenesis, and migration, accelerating skin wound healing. (A) Cell viability of HACAT and HEK293 cells treated with Na$^+$ ionophores (monensin A, nanchangmycin, lasalocid, and salinomycin). (B, C) Cell viability of monensin A-treated PMDF (B, left), MEF (B, right), and HUVEC (C). (D, E) The endothelial tube formation of HUVEC treated with or without monensin A (D). The tube nodes and lengths were quantified using ImageJ (E). Field diameter: 2 mm. (F, G) Representative embryonic blood vessels (F) in chickens chorioallantois model supplemented with monensin A (125 nM) for 24 h. The vessel nodes and lengths were quantified using ImageJ (G). Field diameter: 1 cm. (H) Representative image (left) and quantification (right) of the scratched wound at indicated points in time (0 h and 20 h). Scale bar: 20 μm. (I) Schematic of full-thickness skin wounding and administration regimen on BLAB/c mice. (J) The representative images and wound healing dynamics of BALB/c (n = 5 per group) mice externally administrated with monensin A. (K) H&E staining of healed skin wounds on day 12. The wound width and granulation thickness were quantified using the ImageViewer. Scale bar: 500 μm (left) and 250 μm (right). (L) Immunostaining for the endothelial markers CD31 (green) and α-SMA (red) on the excised skin wound tissues. Scale bar: 500 μm (left) and 100 μm (right). Number of CD31$^+$ or α-SMA$^+$ vessels were accounted by the ImageJ. Data are expressed as mean ± SD (A-C, E, G, and H) or mean ± s.e.m (J, K, and L). One-way ANOVA with Dunnett test (A-C, H, K, L, every mean versus control); two-tailed Student's unpaired *t*-test (E, G); two-way ANOVA with Sidak's multiple comparisons (J). (For interpretation of the references to colour in this figure legend, the reader is referred to the Web version of this article.)

marked reduction in membrane fluidity induced by monensin A in both HACAT and HEK293 cells (Fig. 4E). Thermodynamic analysis through isothermal titration calorimetry (ITC) demonstrated that monensin A titrated against cardiolipin in a salt solution did not exhibit heat absorption or exotherm, indicating a potential lack of a direct binding to cardiolipin, a possibility that contributes to altered membrane fluidity (Fig. S6).

In the context of the Q cycle turnover, the poor IMM fluidity lengthens the half-life of the semiquinone form at the complex III Qo site, leading to an O^{2-} leak at the CoQ site due to reduced CoQH$_2$ diffusion [34,37]. As expected, monensin A induced a burst of ROS in both HACAT and HEK293 cells (Fig. 4F–H). We utilized myxothiazol, a Qo site inhibitor in complex III, to pharmacologically block the quinone redox catalysis. Notably, the inhibitor abrogated ROS production in monensin A-treated HACAT and HEK293 cells (Fig. 4F). Additionally, the ROS scavenger N-acetyl cysteine (NAC) was effective in scavenging monensin A-induced ROS generation (Fig. 4H). Both myxothiazol and NAC mitigated the cell growth induced by monensin A in both HACAT and HEK293 cells (Fig. 4G and I), indicating that ROS is responsible for the cell proliferation-promoting activity of monensin A *in vitro*. In a mouse model of acute skin wounding, NAC intervention attenuated the efficacy of monensin A in wound healing (Fig. 4J), suggesting that ROS is a vital effector in response to monensin A-induced wound closure.

3.6. Monensin A-treated HACAT cells actively express mitochondrial genes

To comprehensively excavate the monensin A-mediated underlying molecular mechanisms, we performed a bulk RNA-sequencing on monensin A-treated HACAT cells. The divergence of gene expression induced by the ionophore was analyzed (Fig. 5A, Figs. S7A–C). Interestingly, pathway enrichment analysis of Gene Ontology (GO) terms revealed a prominent divergence towards genes associated with mitochondrial functions among the top-upregulated pathways (Fig. 5B). The heatmap illustrated the up-regulation of genes implicated in the mitochondrial oxidative phosphorylation system, including complex subunits, mitochondrial tRNA (mtRNA), and rRNA (mrRNA) (Fig. 5C). Validation through PCR-based analysis further confirmed a substantial upregulation of mitochondrial genes induced by monensin A, including subunits of complex I (*MT-ND2, MT-ND3, MT-ND4L, MT-ND5*, and *MT-ND6*), IV (*MT-COX3*), V (*MT-ATP8*), and a ribosomal RNA (*RNR2*) (Fig. 5D).

### 3.7. Monensin A enhances OXPHOS and facilitates healing in diabetic wounds

We further investigated the effect of monensin A on mitochondrial function. A gradual acceleration of oxygen consumption induced by monensin A in HACAT cells was observed (Fig. 6A), even when the incubation time was extended to 24 min (Fig. 6B). Similarly, other Na$^+$ ionophores, including nanchangmycin, lasalocid, and salinomycin, also boosted the oxygen consumption rate (Fig. 6C). The effect of all these Na$^+$ ionophores was mild compared to FCCP that is a robust uncoupling

agent (Fig. 6A–C). In contrast, nigericin, which predominantly transports K$^+$ [32], did not elevate the oxygen consumption of HACAT cells (Fig. 6C). Of note, the mitochondrial membrane potential (MMP) in HACAT cells exposed to these Na$^+$ ionophores, excluding nigericin, exhibited a remarkable hyperpolarization (Fig. 6D). As an effect, monensin A accelerated the glucose consumption rate within 24 h in both HACAT and HEK293 cells (Figs. S8A and B). Additionally, there was an enhancement in mitochondrial ATP production, a vital factor for proliferating cells, with all Na$^+$ ionophores markedly raising intracellular ATP levels in HACAT cells (Fig. 6E). These results unveil additional function of these Na$^+$ ionophores acting as moderate mitochondrial H$^+$ replenishments, thereby augmenting a high-rate electron transfer in the mitochondrial electron transport chain to expedite mitochondrial energy metabolism.

Mitochondrial dysfunction is a hallmark of chronic non-healing wounds in diabetes [38,39]. Since monensin A has an appealing activity on improving mitochondrial energy metabolism, we hypothesized that monensin A may be applicable to facilitate the healing of diabetic chronic wounds. In our *in vitro* experiments, a mal-condition with high glucose (200 mM) was detrimental to the proliferation of epidermal keratinocytes (Fig. 6F). Intriguingly, monensin A effectively alleviated this high glucose-mediated cytostatic effect in HACAT cells (Fig. 6F). We next investigated whether external administration of monensin A benefits hard-to-heal wounds, by utilizing DB/DB mice with diabetes (Figs. S9A and B). Notably, monensin A markedly facilitated wound healing at the middle and late stages (16–24 days) in this model (Fig. 6G and H). Consistent with this result, histological examination of excisional wounds in mice that received monensin A displayed minor gap, with a thicker overall tissue compared with that of sham treatment (Fig. 6I). Of note, in the adverse high-glucose microenvironment, monensin A still remarkably promoted angiogenesis at the healing site (Fig. 6J). At the wound healing site receiving monensin A treatment, we observed a higher deposition of collagen matrix (Fig. S10). These results collectively suggest that the external administration of monensin A can expedite wound healing dynamics in mouse models, particularly in chronic wounds with diabetes.

4. Discussion

The biological function described to Na$^+$ is traditionally restricted to act as a mediator of membrane potential and osmotic equilibrium. Herein, we prove a new role of Na$^+$ that serving as a determinant factor in skin wound healing. Furthermore, we provide compelling evidence that the concurrent supplementation of mitochondrial Na$^+$ and H$^+$ induced by Na$^+$ ionophores (monensin A, nanchangmycin, lasalocid, and salinomycin) is integral to mobilize productive wound healing programs. Mechanistically, the elevated mitochondrial Na$^+$ induced by these ionophores interacts with phospholipids, subsequently decelerating inner mitochondrial membrane fluidity to enhance ROS generation at mitochondrial complex III fluidity (Fig. 7) [34,35]. We identified ROS as a vital effector on Monensin A-induced acute skin wound healing. Additionally, the Na$^+$ ionophores-mediated mitochondrial H$^+$ supplementary drives mitochondrial energy production, providing
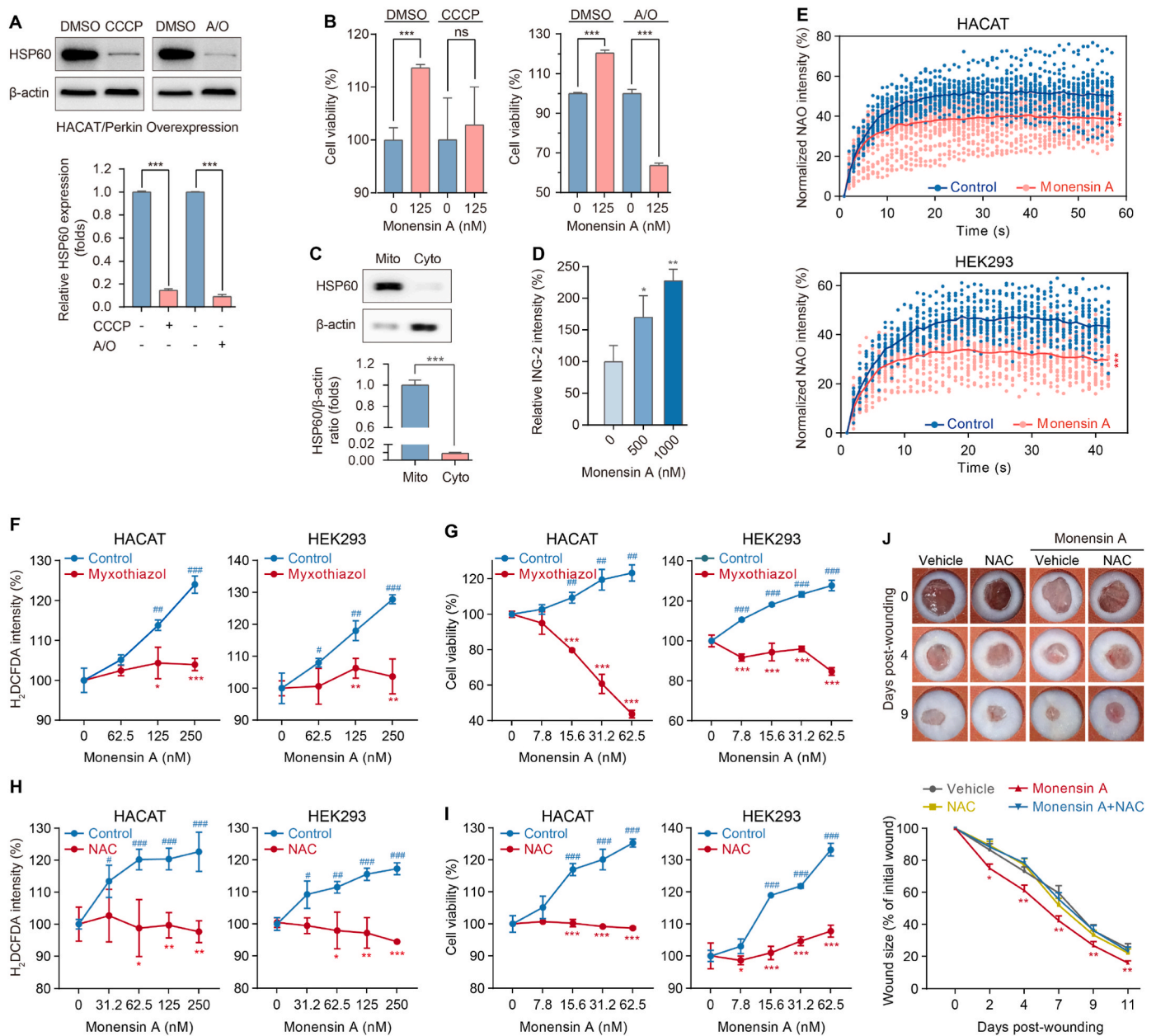
Fig. 4. Monensin A increases mitochondrial Na$^+$ content and attenuates the IMM fluidity to drive ROS generation, a key effector in acute wound healing. (A) The expression of HSP60 in the Perkin overexpressed HACAT cells under CCCP or antimycin A plus oligomycin A (A/O) treatment. (B) Effect of mitochondria depletion on monensin A-mediated proliferation in Perkin-transfected HACAT cells treated with inducers (CCCP or A/O). (C) The validation of the extracted mitochondria derived from HACAT cells via comparing the expression of HSP60 and β-actin between mitochondrial pellets (mito) and cytoplasmic supernatant (cyto). (D) Na$^+$ levels in extracted mitochondria pellets incubated with monensin A for 0.5 h. (E) NAO FRAP of HACAT (control, n = 22 points; monensin A, n = 37 points) and HEK293 (control, n = 23 points; monensin A, n = 27 points) cells exposed to monensin A (125 nM) for 1 h. Statistical significance between the two groups at the last time point was analyzed. (F, H) Quantification of intracellular ROS levels in HACAT and HEK293 cells treated with monensin A in combination with myxothiazol (F) or NAC (H). (G, I) Cell viability of HACAT and HEK293 cells treated with monensin A in combination with myxothiazol (G) or NAC (I). (J) Epidermal wounds (up) and their healing dynamics (down) in BALB/c mice (n = 5 per group) externally administrated with monensin A (125 nM) in the presence or absence of NAC (20 mM). Error bars are mean ± SD (A-D, and F–I) or mean ± s.e.m (J). Two-tailed Student's unpaired *t*-test (A, C, E; last time point between two groups in E); one-way ANOVA with Dunnett test (B, D; every mean versus control); two-way ANOVA with Sidak's multiple comparisons (F–J).

comprehensive support for the wound repair process (Fig. 7). These newly identified mechanisms represent a novel strategy that can be employed to enhance the plasticity of skin wounds, particularly in the context of chronic wounds associated with diabetes mellitus.

Hyponatremia, defined as a serum Na$^+$ concentration below 135 mmol/L, stands as the most common electrolyte abnormality, with an estimated prevalence of 1.72 % in the US population [40]. Its prevalence is notably higher among hospitalized patients, ranging from 15 to 20 % [41,42], and is linked to increased mortality [43]. Of note,

hyponatremia has not been reported to be associated with injury repair. Our study provides firsthand data highlighting a distinctive characteristic of impaired healing in skin wounds under hyponatremic conditions. This discovery underscores the importance of additional care and treatment for the hard-to-heal wounds in patients with hyponatremia. Furthermore, Na$^+$ ionophores, such as monensin A, nanchangmycin, lasalocid, and salinomycin, emerge as a potential therapeutic candidates tailored to address such cases.

We devised an intervention strategy to moderately elevate the
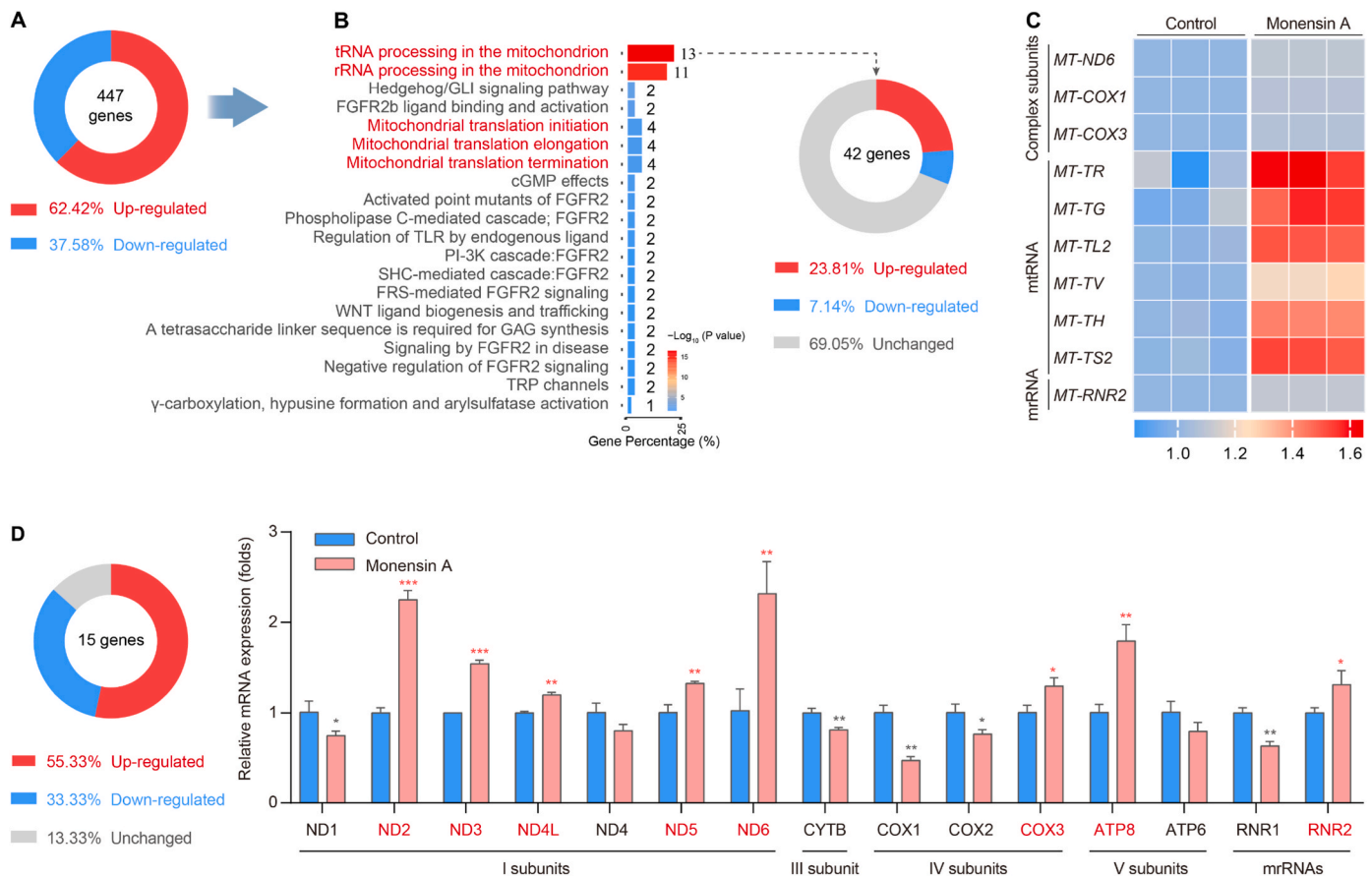
Fig. 5. Monensin An up-regulates mitochondrially encoded genes. (A) Overview of the monensin A mediated alteration of gene expression on HACAT cells using bulk RNA-seq. (B) Pathway enrichment analysis arranging the top up-regulated pathways according to the adjusted p-value (left). The altered information on the top-ranking pathway was further excavated (right). (C) Heatmap shows monensin A-triggered actively expressed genes involved in the top-ranking pathway. Data are color-coded to reflect the relative expression level of mitochondrially encoded genes. All data are normalized to their matched control. (D) PCR-based validation of the mRNA expression of mitochondrial genes in HACAT cells treated with or without monensin A (125 nM) for 3 h. Data are represented as mean ± SD. Two-tailed Student's unpaired *t*-test (D). (For interpretation of the references to colour in this figure legend, the reader is referred to the Web version of this article.)

mitochondrial Na^+ and H^+ levels to stimulate wound repair by utilizing Na^+ ionophores. These ionophores possess the unique ability to reversibly bind Na^+ and H^+, forming lipid-soluble complexes that can freely penetrate across lipid bilayer [44]. Notably, the well-known Na^+ ionophores, such as monensin A, lasalocid, and salinomycin, have been extensively utilized in veterinary practice for controlling coccidiosis. Their effectiveness in this application is closely tied to their capacity to bind and transport Na^+ across cell membranes [45]. Monensin A, a representative polyether ionophore, is an intermediate biosynthetic metabolite produced by *Streptomyces cinnamonensis* bacteria. The affinity of monensin A binding monovalent metal cations in the order of $Na^+>K^+>Li^+>Rb^+>Cs^+$ [46]. Nanchangmycin (dianemycin), produced by *Streptomyces nanchangensis NS3226*, shares homologous biosynthetic gene clusters and similar chemical structure with monensin A, demonstrating a preference for binding to Na^+ and forming a flexible and adaptable metal complex [47,48]. Lasalocid, isolated from *Streptomyces lasaliensis*, preferentially transports Na^+ across lipid bilayers [28]. Salinomycin, another ionophore, can transport Na^+ and K^+ into the cytoplasm [28,49]. Nigericin, a well-known K^+ ionophore with a substantially stronger affinity for K^+ than Na^+ ($K^+>Rb^+>Cs^+\gg Na^+$) [50], was employed in this study as a non-sodium ion carrier. Within the mitochondrial matrix, the balance of Na^+ is governed by the Na^+/Ca^{2+} exchanger (influx) and Na^+/H^+ exchanger (efflux) located in the mitochondrial membrane [51]. This trade-off dynamic model maintains a relatively low Na^+ environment in the mitochondrial matrix, with approximately 8 folds lower than extramitochondrial Na^+ [52]. We thus

employed Na^+ ionophores as transporters to equilibrate the Na^+ gradient in the mitochondrial matrix. In the monensin A-mediated Na^+ antiport, it has been found to concomitantly transport H^+, with monensin A-sodium and monensic acid coexisting in a 1:1 ratio [53,54]. Consequently, we found here that the dually supplementing with Na^+ and H^+ within the mitochondrial matrix leads to a notable improvement in mitochondrial energy metabolism. Of note, monensin A is non-genotoxic and non-carcinogenic based on the chronic carcinogenicity studies performed in rats and mice [55]. The intake of monensin sodium derived from meat is safe for the consumer, according to a report from the European Food Safety Authority [55]. Hence, this Na^+ ionophore shows promise as a controlled pharmacological approach to foster damaged skin repair, which is likely to be a safe, feasible, and economical therapy.

In this study, we have attempted to establish the relationship between the Na^+ ionophores-mediated up-regulation of Na^+ level and its corresponding cell proliferation. However, we have to confront a fact that the increase of intracellular Na^+ levels in HACAT and HEK293 cells treated with low concentrations (<31.25 nM) of Na^+ ionophores are unable to be detected by the probe ING-2. For the underlying reason, we suppose here that the treatment with low concentrations of Na^+ ionophores cause little fluctuation in intracellular Na^+ levels, this subtle change is unable to be measured due to the limited sensitivity of the Na^+ probe. At least, we confirmed that Na^+ ionophores are capable to transport Na^+ into cells. Therefore, it is a reasonable speculation that, even at low concentrations (<31.25 nM), Na^+ ionophores can transport
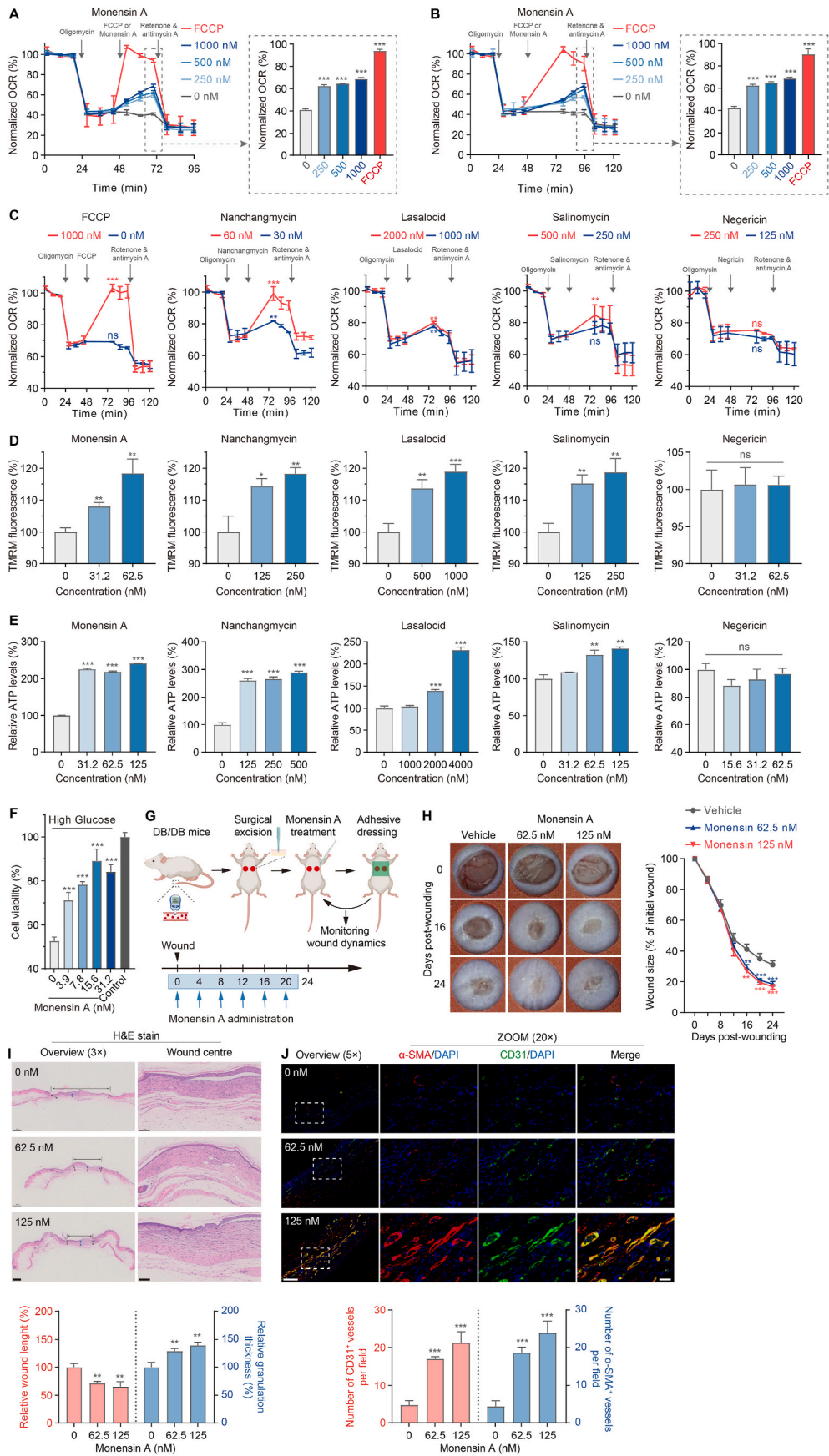
(caption on next page)

Fig. 6. Na^+ ionophores act as protonophores to stimulate mitochondrial electron translation and energy generation. (A, B) Oxygen consumption rate (OCR) in HACAT cells treated with monensin A or FCCP at the excitation phase (A). Monensin A treatment was prolonged to 24 min (B). Statistical significance of the OCR between the stimulators (monensin A and FCCP) and control was independently calculated on the right side. (C) OCR of HACAT cells with a prolonged incubation (24 min) of other ionophores (nanchangmycin, lasalocid, salinomycin, and nigericin) or FCCP. The significance between the previous (at 48 min time point) and post (at 72 min time point) excitation was statistically analyzed. (D) TMRM (20 nM) indicated mitochondrial membrane potential in HACAT cells incubated with ionophores for 3 h. (E) Intracellular ATP levels in HACAT cells treated with ionophores for 24 h. (F) Cell viability of HACAT cells cultured in the completed DMEM medium supplemented with high glucose (200 mM), and monensin A treatment was employed for 72 h. (G) Schematic of full-thickness skin wounding and dosage regimen on diabetic DB/DB mice. (H) The representative images (left) and wound healing dynamics (right) of DB/DB mice (vehicle, n = 7; monensin A-treated groups, n = 8) treated with monensin A. (I) H&E staining of the wound tissues excised on day 24. The width and granulation thickness of the skin wounds in pathological sections were quantified using the ImageViewer. Scale bar: 500 μm (left) and 250 μm (right). (J) Immunostaining for the endothelial markers CD31 (green) and α-SMA (red) on full-thickness skin wound tissues. Scale bar: 500 μm (left) and 100 μm (right). Number of the $CD31^+$ or $\alpha\text{-}SMA^+$ vessels were quantified using the ImageJ. Data are expressed as mean ± SD (A–F) or mean ± s.e.m (H–J). One-way ANOVA with Dunnett test (A, B, D-F, I, and J, every mean versus control); two-tailed Student's unpaired *t*-test (C); two-way ANOVA with Sidak's multiple comparisons (H). (For interpretation of the references to colour in this figure legend, the reader is referred to the Web version of this article.)
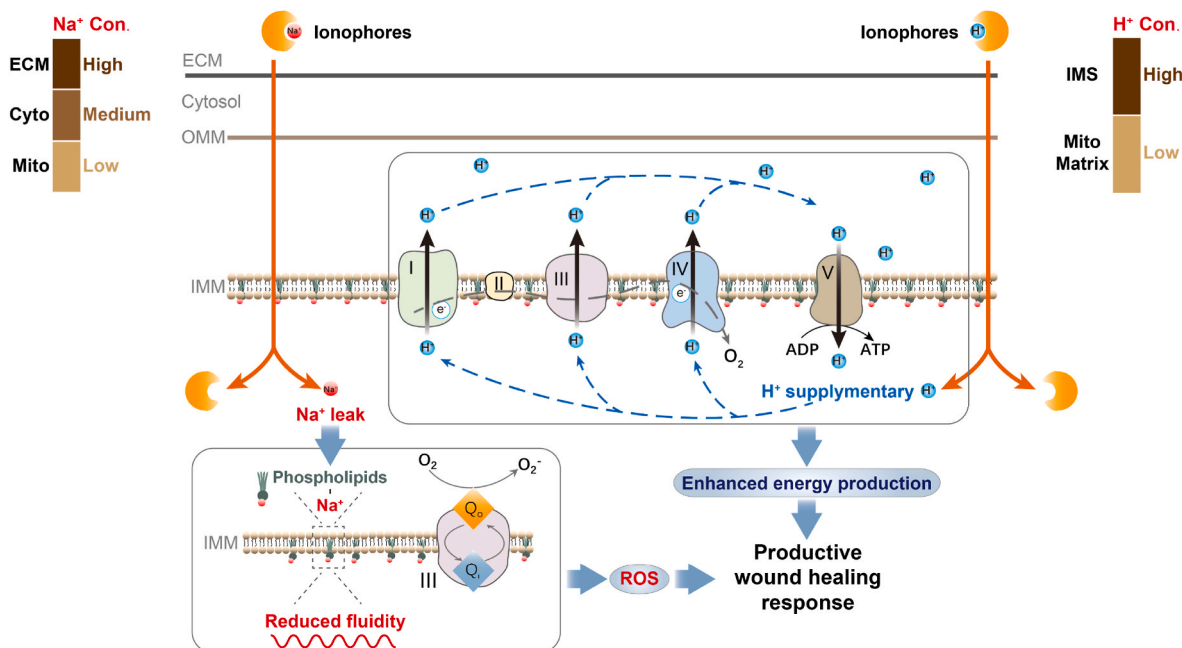
Fig. 7. Scheme of the Na^+ ionophores-mediated molecular pathways driving ROS generation and mitochondrial energy metabolism to favor a productive wound healing program. Mechanistically, Na^+ ionophores carrying Na^+ and H^+ penetrate freely across plasma and mitochondrial membranes, simultaneously increasing Na^+ and H^+ levels within the mitochondrial matrix. Mitochondrial Na^+ binds to phospholipids located in the IMM, restraining the fluidity of the inner leaflet membrane to decrease $CoQH_2$ diffusion in complex III, consequently boosting ROS production at the Qo site. On the other side, the supplementary of H^+ enforces mitochondrial OXPHOS, driving ATP production. The cumulative outcome of the Na^+ ionophores-driven ROS and OXPHOS yields favorable wound repair via facilitating reepithelization, migration, and angiogenesis. ECM: extracellular matrix; Cyto: cytosol; Mito: mitochondrion; IMS: mitochondrial intermembrane space; Mito matrix: mitochondrial matrix.

a certain amount of Na^+ into cells to persistently stimulate the function of wound-repairing cells. In the mice wound healing experiments, two monensin A groups of 62.5 nM and 125 nM demonstrated similar wound healing efficacy. We speculate that the two doses may locate at the plateau of the dose-stimulation curve. Along the way, a dose of monensin A less than 62.5 nM should be chosen in future dose-response animal study.

The mitochondrion, an organelle ubiquitous in most eukaryotic cells, primarily functions to generate metabolic energy in the form of ATP, playing a critical role in maintaining cellular and tissular homeostasis [56,57]. It serves as a master dispatch center for supporting energy and signaling in repair programs, empowering repair cells to retaliate against adverse stress. In patients with type 2 diabetes mellitus, pathological shifts in fuel metabolism and energy substrate consumption contribute to mitochondrial dysfunction and mitochondrial DNA depletion across organ systems [58,59]. Pathophysiologically, insulin resistance or deficiency is characterized by inefficient mitochondrial coupling [60]. In this study, as a result of moderate H^+ leak across mitochondrial inner membrane by employing Na^+ ionophores, the pace

of mitochondrial metabolism will be accelerated to restore the physiological function of wound-repairing cells in severely high-glucose microenvironments. Our experimental results feature an overall enhancement of mitochondrial functions in keratinocytes under the treatment of Na^+ ionophores. Monensin A, in particular, demonstrates a collective potentiation of mitochondrial gene expression, mtDNA copy number, oxygen consumption, glucose utilization, and ATP production. This versatile agent confers a comprehensive improvement in mitochondrial energy metabolism to support wound healing programs. Consequently, the robust acceleration of epidermal wound closure has been yielded in diabetic mice following external administration of the agent, indicating that this Na^+ ionophore may offer a suitable remedy for the intractable complications associated with mitochondrial dysfunction caused by metabolic disorders in diabetes.

5. Conclusions

In sum, we reveal that Na^+ is a determinant factor in skin wound healing. The Na^+ ionophores-triggered dual supplementation of Na^+

and H^+ within the mitochondrial matrix compels ROS generation and energy metabolism, ultimately favoring productive wound healing programs. Given that the scarcity of available medicines for the treatment of intractable chronic wounds in diabetes, our study lays a foundation for the development of Na^+ ionophores as first-in-class candidates for wound care in individuals with diabetic wounds.

Ethics statement

All animal experiments were approved by the Sun Yat-sen University Institutional Animal Care and Use Committee (No. IACUC-2019111301, IACUC-2019111403, and IACUC-2020121401). All animal experimental contents were complied with the WMA Statement on animal use in biomedical research.

CRediT authorship contribution statement

Liangliang Bai: Investigation, Formal analysis, Data curation. **Linping Wu:** Writing – review & editing. **Changsheng Zhang:** Resources. **Zhiwen Liu:** Resources. **Liang Ma:** Resources. **Jing Ni:** Investigation. **Dezhen He:** Investigation. **Mingxuan Zhu:** Investigation. **Shaoyong Peng:** Resources. **Xiaoxia Liu:** Funding acquisition. **Huichuan Yu:** Funding acquisition, Data curation. **Yuhe Lei:** Resources. **Yanxin Luo:** Writing – review & editing, Funding acquisition. **Yu Zhang:** Funding acquisition. **Xiaolin Wang:** Writing – review & editing, Project administration. **Gang Wei:** Writing – review & editing. **Yingjie Li:** Writing – review & editing, Writing – original draft, Funding acquisition.

Declaration of competing interest

The authors declare that they have no known competing financial interests or personal relationships that could have appeared to influence the work reported in this paper.

Data availability

Data will be made available on request.

Acknowledgments

Appendix A. Supplementary data

Supplementary data to this article can be found online at https://doi.org/10.1016/j.mtbio.2024.101056.

References

[1] K. McDermott, M. Fang, A.J.M. Boulton, E. Selvin, C.W. Hicks, Etiology, epidemiology, and disparities in the burden of diabetic foot ulcers, Diabetes Care 46 (1) (2022) 209–221.

[2] D.G. Armstrong, T.W. Tan, A.J.M. Boulton, S.A. Bus, Diabetic foot ulcers: a review, JAMA 330 (1) (2023) 62–75.

[3] F. Werdin, M. Tenenhaus, H.O. Rennekampff, Chronic wound care, Lancet 372 (9653) (2008) 1860–1862.

[4] E. Eriksson, P.Y. Liu, G.S. Schultz, M.M. Martins-Green, R. Tanaka, D. Weir, et al., Chronic wounds: treatment consensus, Wound Repair Regen. 30 (2) (2022) 156–171.

[5] D.G. Armstrong, A.J.M. Boulton, S.A. Bus, Diabetic foot ulcers and their recurrence, N. Engl. J. Med. 376 (24) (2017) 2367–2375.

[6] F. Chang, N. Minc, Electrochemical control of cell and tissue polarity, Annu. Rev. Cell Dev. Biol. 30 (2014) 317–336.

[7] S. Chen, W. Cui, Z. Chi, Q. Xiao, T. Hu, Q. Ye, et al., Tumor-associated macrophages are shaped by intratumoral high potassium via Kir2.1, Cell Metabol. 34 (11) (2022) 1843–1859.e11.

[8] M. Levin, Bioelectric signaling: reprogrammable circuits underlying embryogenesis, regeneration, and cancer, Cell 184 (8) (2021) 1971–1989.

[9] A.S. Tseng, W.S. Beane, J.M. Lemire, A. Masi, M. Levin, Induction of vertebrate regeneration by a transient sodium current, J. Neurosci. 30 (39) (2010) 13192–13200.

[10] L.F. George, S.J. Pradhan, D. Mitchell, M. Josey, J. Casey, M.T. Belus, et al., Ion channel contributions to wing development in *Drosophila melanogaster*, G3 (Bethesda) 9 (4) (2019) 999–1008.

[11] A.M. Bertholet, Y. Kirichok, Mitochondrial H^+ leak and thermogenesis, Annu. Rev. Physiol. 84 (2022) 381–407.

[12] J.G. Geisler, 2, 4 Dinitrophenol as medicine, Cells 8 (3) (2019) 280.

[13] R.J. Perry, D.Y. Zhang, X.M. Zhang, J.L. Boyer, G.I. Shulman, Controlled-release mitochondrial protonophore reverses diabetes and steatohepatitis in rats, Science 347 (6227) (2015) 1253–1256.

[14] S. Rovira-Llopis, C. Bañuls, N. Diaz-Morales, A. Hernandez-Mijares, M. Rocha, V. M. Victor, Mitochondrial dynamics in type 2 diabetes: pathophysiological implications, Redox Biol. 11 (2017) 637–645.

[15] N. Liu, H. Matsumura, T. Kato, S. Ichinose, A. Takada, T. Namiki, et al., Stem cell competition orchestrates skin homeostasis and ageing, Nature 568 (7752) (2019) 344–350.

[16] Z. Zhang, I. Bothe, F. Hirche, M. Zweers, D. Gullberg, G. Pfitzer, et al., Interactions of primary fibroblasts and keratinocytes with extracellular matrix proteins: contribution of alpha2beta1 integrin, J. Cell Sci. 119 (Pt 9) (2006) 1886–1895.

[17] C. Correia-Melo, G. Ichim, S.W. Tait, J.F. Passos, Depletion of mitochondria in mammalian cells through enforced mitophagy, Nat. Protoc. 12 (1) (2017) 183–194.

[18] Y. Li, L. Bai, H. Yu, D. Cai, X. Wang, B. Huang, et al., Epigenetic inactivation of α-internexin accelerates microtubule polymerization in colorectal cancer, Cancer Res. 80 (23) (2020) 5203–5215.

[19] M. Zhu, L. Bai, X. Liu, S. Peng, Y. Xie, H. Bai, et al., Silence of a dependence receptor CSF1R in colorectal cancer cells activates tumor-associated macrophages, J. Immunother Cancer 10 (12) (2022) e005610.

[20] P. Tao, Y. Kuang, Y. Li, W. Li, Z. Gao, L. Liu, et al., Selection of a full agonist combinatorial antibody that rescues Leptin deficiency in vivo, Adv. Sci. 7 (16) (2020) 2000818.

[21] P. Nowak-Sliwinska, T. Segura, M.L. Iruela-Arispe, The chicken chorioallantoic membrane model in biology, medicine and bioengineering, Angiogenesis 17 (4) (2014) 779–804.

[22] S. Peng, Y. Li, M. Huang, G. Tang, Y. Xie, D. Chen, et al., Metabolomics reveals that CAF-derived lipids promote colorectal cancer peritoneal metastasis by enhancing membrane fluidity, Int. J. Biol. Sci. 18 (5) (2022) 1912–1932.

[23] N. Yao, Y. Li, Y. Lei, N. Hu, W. Chen, Z. Yao, et al., A piperazidine derivative of 23-hydroxy betulinic acid induces a mitochondria-derived ROS burst to trigger apoptotic cell death in hepatocellular carcinoma cells, J. Exp. Clin. Cancer Res. 35 (1) (2016) 192.

[24] K.P. Krafts, Tissue repair: the hidden drama, Organogenesis 6 (4) (2010) 225–233.

[25] S.E. Iismaa, X. Kaidonis, A.M. Nicks, N. Bogush, K. Kikuchi, N. Naqvi, et al., Comparative regenerative mechanisms across different mammalian tissues, NPJ Regen Med 3 (2018) 6.

[26] J. Berlanga-Acosta, J. Gavilondo-Cowley, P. López-Saura, T. González-López, M. D. Castro-Santana, E. López-Mola, et al., Epidermal growth factor in clinical practice - a review of its biological actions, clinical indications and safety implications, Int. Wound J. 6 (5) (2009) 331–346.

[27] X. Wan, F. Gen, Y. Sheng, M. Ou, F. Wang, T. Peng, et al., Meta-analysis of the effect of Kangfuxin Liquid on diabetic patients with skin ulcers, Evid. Based Complement. Alternat. Med. 2021 (2021) 1334255.

[28] J. Rutkowski, B. Brzezinski, Structures and properties of naturally occurring polyether antibiotics, BioMed Res. Int. 2013 (2013) 162513.

[29] W. Li, J.Y. Chen, C. Sun, R.P. Sparks, L. Pantano, R.U. Rahman, et al., Nanchangmycin regulates FYN, PTK2, and MAPK1/3 to control the fibrotic activity of human hepatic stellate cells, Elife 11 (2022) e74513.

[30] M. Antoszczak, A comprehensive review of salinomycin derivatives as potent anticancer and anti-CSCs agents, Eur. J. Med. Chem. 166 (2019) 48–64.

[31] A. Huczyński, Polyether ionophores-promising bioactive molecules for cancer therapy, Bioorg. Med. Chem. Lett. 22 (23) (2012) 7002–7010.

[32] G. Xu, S. Fu, X. Zhan, Z. Wang, P. Zhang, W. Shi, et al., Echinatin effectively protects against NLRP3 inflammasome-driven diseases by targeting HSP90, JCI Insight 6 (2) (2021) e134601.

[33] R.D.S. Marques, R.F. Cooke, Effects of ionophores on ruminal function of beef cattle, Animals 11 (10) (2021) 2871.

[34] P. Hernansanz-Agustín, C. Choya-Foces, S. Carregal-Romero, E. Ramos, T. Oliva, T. Villa-Piña, et al., Na^+ controls hypoxic signalling by the mitochondrial respiratory chain, Nature 586 (7828) (2020) 287–291.

[35] E. Deplazes, J. White, C. Murphy, C.G. Cranfield, A. Garcia, Competing for the same space: protons and alkali ions at the interface of phospholipid bilayers, Biophys. Rev. 11 (3) (2019) 483–490.

[36] S.E. Horvath, G. Daum, Lipids of mitochondria, Prog. Lipid Res. 52 (4) (2013) 590–614.

[37] M. Sarewicz, A. Osyczka, Electronic connection between the quinone and cytochrome C redox pools and its role in regulation of mitochondrial electron transport and redox signaling, Physiol. Rev. 95 (1) (2015) 219–243.

[38] M.V. Pinti, G.K. Fink, Q.A. Hathaway, A.J. Durr, A. Kunovac, J.M. Hollander, Mitochondrial dysfunction in type 2 diabetes mellitus: an organ-based analysis, Am. J. Physiol. Endocrinol. Metab. 316 (2) (2019) E268–E285.

[39] J.G. Powers, C. Higham, K. Broussard, T.J. Phillips, Wound healing and treating wounds: chronic wound care and management, J. Am. Acad. Dermatol. 74 (4) (2016) 607–625.

[40] S. Mohan, S. Gu, A. Parikh, J. Radhakrishnan, Prevalence of hyponatremia and association with mortality: results from NHANES, Am. J. Med. 126 (12) (2013) 1127–11237.e1.

[41] J. Hao, Y. Li, X. Zhang, C. Pang, Y. Wang, S.U. Nigwekar, et al., The prevalence and mortality of hyponatremia is seriously underestimated in Chinese general medical patients: an observational retrospective study, BMC Nephrol. 18 (1) (2017) 328.

[42] L. Holland-Bill, C.F. Christiansen, U. Heide-Jørgensen, S.P. Ulrichsen, T. Ring, J. O. Jørgensen, et al., Hyponatremia and mortality risk: a Danish cohort study of 279 508 acutely hospitalized patients, Eur. J. Endocrinol. 173 (1) (2015) 71–81.

[43] S.S. Waikar, D.B. Mount, G.C. Curhan, Mortality after hospitalization with mild, moderate, and severe hyponatremia, Am. J. Med. 122 (9) (2009) 857–865.

[44] J. Rutkowski, B. Brzezinski, Structures and properties of naturally occurring polyether antibiotics, BioMed Res. Int. 31 (2013).

[45] V.M. Dembitsky, Natural polyether ionophores and their pharmacological profile, Mar. Drugs 20 (5) (2022) 292.

[46] T. Dudev, D. Cheshmedzhieva, R. Dimitrova, P. Dorkov, I. Pantcheva, Factors governing the competition between group IA and IB cations for monensin A: a DFT/PCM study, RSC Adv. 10 (10) (2020) 5734–5741.

[47] L.K. Steinrauf, E.W. Czerwinski, M. Pinkerton, Comparison of the monovalent cation complexes of monensin, nigericin, and dianemycin, Biochem. Biophys. Res. Commun. 45 (5) (1971) 1279–1283.

[48] Q. Yu, A. Du, T. Liu, Z. Deng, X. He, The biosynthesis of the polyether antibiotic nanchangmycin is controlled by two pathway-specific transcriptional activators, Arch. Microbiol. 194 (6) (2012) 415–426.

[49] F.G. Riddell, S.J. Tompsett, The transport of Na^+ and K^+ ions through phospholipid bilayers mediated by the antibiotics salinomycin and narasin studied by ^{23}Na- and ^{39}K-NMR spectroscopy, Biochim. Biophys. Acta 1024 (1) (1990) 193–197.

[50] S. Mariathasan, D.S. Weiss, K. Newton, J. McBride, K. O'Rourke, M. Roose-Girma, et al., Cryopyrin activates the inflammasome in response to toxins and ATP, Nature 440 (7081) (2006) 228–232.

[51] E. Murphy, D.A. Eisner, Regulation of intracellular and mitochondrial sodium in health and disease, Circ. Res. 104 (3) (2009) 292–303.

[52] D.W. Jung, L.M. Apel, G.P. Brierley, Transmembrane gradients of free Na^+ in isolated heart mitochondria estimated using a fluorescent probe, Am. J. Physiol. 262 (4 Pt 1) (1992) C1047–C1055.

[53] A. Huczyński, J. Janczak, D. Lowicki, B. Brzezinski, Monensin A acid complexes as a model of electrogenic transport of sodium cation, Biochim. Biophys. Acta 1818 (9) (2012) 2108–2119.

[54] K. Nakazato, Y. Hatano, Monensin-mediated antiport of Na^+ and H^+ across liposome membrane, Biochim. Biophys. Acta 1064 (1) (1991) 103–110.

[55] V. Bampidis Feedap, G. Azimonti, M.d.L. Bastos, H. Christensen, B. Dusemund, et al., Safety and efficacy of Elancoban® G200 (monensin sodium) for chickens for fattening, chickens reared for laying and turkeys, EFSA J. 17 (12) (2019) e05891.

[56] J.J. Collier, M. Oláhová, T.G. McWilliams, R.W. Taylor, Mitochondrial signalling and homeostasis: from cell biology to neurological disease, Trends Neurosci. 46 (2) (2023) 137–152.

[57] J. Zhou, L. Xu, X. Duan, W. Liu, X. Zhao, X. Wang, et al., Large-scale RNAi screen identified Dhpr as a regulator of mitochondrial morphology and tissue homeostasis, Sci. Adv. 5 (9) (2019) eaax0365.

[58] G.N. Ruegsegger, A.L. Creo, T.M. Cortes, S. Dasari, K.S. Nair, Altered mitochondrial function in insulin-deficient and insulin-resistant states, J. Clin. Invest. 128 (9) (2018) 3671–3681.

[59] C. Huang, L. Chen, J. Li, J. Ma, J. Luo, Q. Lv, et al., Mitochondrial DNA copy number and risk of diabetes mellitus and metabolic syndrome, J. Clin. Endocrinol. Metab. (2023) e406–e417.

[60] G.N. Ruegsegger, A.L. Creo, T.M. Cortes, S. Dasari, K.S. Nair, Altered mitochondrial function in insulin-deficient and insulin-resistant states, J. Clin. Invest. 128 (9) (2018) 3671–3681.